

Three-Dimensional Root Phenotyping with a Novel Imaging and Software Platform^{1[C][W][OA]}

Randy T. Clark, Robert B. MacCurdy, Janelle K. Jung, Jon E. Shaff, Susan R. McCouch, Daniel J. Aneshansley, and Leon V. Kochian*

Department of Biological and Environmental Engineering (R.T.C., D.J.A.), Robert W. Holley Center for Agriculture and Health, United States Department of Agriculture-Agricultural Research Service (R.T.C., J.E.S., L.V.K.), Department of Mechanical and Aerospace Engineering (R.B.M.), and Department of Plant Breeding and Genetics (J.K.J., S.R.M.), Cornell University, Ithaca, New York 14853

A novel imaging and software platform was developed for the high-throughput phenotyping of three-dimensional root traits during seedling development. To demonstrate the platform's capacity, plants of two rice (*Oryza sativa*) genotypes, Azucena and IR64, were grown in a transparent gellan gum system and imaged daily for 10 d. Rotational image sequences consisting of 40 two-dimensional images were captured using an optically corrected digital imaging system. Three-dimensional root reconstructions were generated and analyzed using a custom-designed software, RootReader3D. Using the automated and interactive capabilities of RootReader3D, five rice root types were classified and 27 phenotypic root traits were measured to characterize these two genotypes. Where possible, measurements from the three-dimensional platform were validated and were highly correlated with conventional two-dimensional measurements. When comparing gellan gum-grown plants with those grown under hydroponic and sand culture, significant differences were detected in morphological root traits ($P < 0.05$). This highly flexible platform provides the capacity to measure root traits with a high degree of spatial and temporal resolution and will facilitate novel investigations into the development of entire root systems or selected components of root systems. In combination with the extensive genetic resources that are now available, this platform will be a powerful resource to further explore the molecular and genetic determinants of root system architecture.

Root system architecture (RSA) and development has received an increased amount of attention due to advances in phenotyping capabilities and growing insight into the genetic control of root growth (Liu et al., 2005; Tuberosa and Salvi, 2006; de Dorlodot et al., 2007; Armengaud et al., 2009). Previous studies have shown that external factors can affect root morphology and architecture and that root systems have an innate ability to respond and adapt to their rooting environment (Malamy, 2005). Additionally, many reports indicate that certain root qualities in crop plants can help enhance productivity in resource-limited environments due to improved nutrient and water scavenging abilities (Liao et al., 2001; Zhu et al., 2005; Ribaut et al., 2009). Identifying, evaluating, and selectively introducing both intrinsic and environmentally responsive

root architectural characteristics into breeding programs may be a promising area for improving crop production on resource-limited agricultural systems (de Dorlodot et al., 2007).

Elucidating the genetic and developmental basis of RSA presents many challenges that must be addressed through a combination of field-, greenhouse-, and laboratory-based approaches. Field studies provide the "ground truth" about plant growth in a particular environment, but these types of root studies are hindered by intensive excavation processes that destructively sample root systems at a single point during development (Smit, 2000). Furthermore, heterogeneity within and along the soil profile (Lynch, 1995), combined with physical and chemical interactions between various components of the rhizosphere, can drastically impact RSA, even under presumably controlled situations (Ward et al., 2008; Shaff et al., 2009).

The overwhelming variety and complexity of field environments combined with the high responsiveness of root systems make it difficult to obtain precise information about the genetic components of RSA and developmental root traits under field conditions and has consequently led many researchers to pursue predictive practices (Hochholdinger and Tuberosa, 2009). Predictive techniques provide insight about root systems by extrapolating root information from soil cores and root crowns of field-grown plants (Trachsel et al., 2011) or from plants grown in controlled growth systems including hydroponic, pouch,

¹ This work was supported by the National Science Foundation (Plant Genome grant nos. DBI-0820624 and DBI-0606461 as well as Generation Challenge Program grant no. G3008.02).

* Corresponding author; e-mail lvk1@cornell.edu.

The author responsible for distribution of materials integral to the findings presented in this article in accordance with the policy described in the Instructions for Authors (www.plantphysiol.org) is: Leon V. Kochian (lvk1@cornell.edu).

^[C] Some figures in this article are displayed in color online but in black and white in the print edition.

^[W] The online version of this article contains Web-only data.

^[OA] Open Access articles can be viewed online without a subscription.

www.plantphysiol.org/cgi/doi/10.1104/pp.110.169102

pot, and plate systems. In situ methods involving rhizotron, magnetic resonance, and computed tomography techniques have also been developed to facilitate nondestructive spatial and temporal investigations into root systems grown in soil (Taylor et al., 1990; Gregory et al., 2003; Tracy et al., 2010); however, the current scale, resolution, throughput, and cost efficiency of these techniques limit their utility. Additionally, simulation and modeling studies that integrate rhizosphere and growth data help form links between predictive techniques and field studies, allowing researchers to strategically predict, evaluate, and target beneficial root traits or genotypes for specific growth environments (Berntson, 1994; Ho et al., 2004; de Dorlodot et al., 2007).

As a complementary tool to other predictive techniques, gellan gum growth systems with superior optical clarity have been introduced to facilitate non-invasive two-dimensional (2D; Iyer-Pascuzzi et al., 2010) and three-dimensional (3D; Fang et al., 2009) imaging and temporal studies of plant root systems while also allowing reproducible control of the rhizosphere. These recent studies demonstrate the use of gellan gum systems and discuss their enormous potential for high-throughput root phenotyping and novel trait discovery when working with 2D image sets; however, efforts to expand these investigations into the 3D structure remain constrained by low throughput that requires over 1 h to acquire a single root system, small scanning volumes, and limited quantification capabilities.

In this paper, we introduce a novel 3D imaging and software platform to investigate rice (*Oryza sativa*) root system development and quantify RSA of plants grown in a gellan gum system (Fig. 1). This highly versatile phenotyping platform greatly improves throughput and reduces root system capture times to less than 5 min, while also advancing our phenotyping capacity beyond 2D whole root system traits into a range of 3D RSA and root type-specific traits.

RESULTS

RootReader3D Reconstruction and Analysis Software

To process and analyze the images captured with the 3D imaging system (Fig. 1, A and C), custom software was written in the Java programming language (Sun Microsystems) that reconstructs 3D root system models from 2D image sequences and quantifies 3D root system traits. This software, RootReader3D, utilizes a silhouette-based back-projection algorithm (Mulayim et al., 2003; Zhu et al., 2006) combined with cross-sectional volume segmentation to generate 3D root models (Supplemental Fig. S1). It adopts a template-matching technique (Kalman and Attila, 1999), followed by a valence-driven spatial median filter to generate unit-width skeleton representations of the root models (Wang and Cheng, 2008). Various viewing

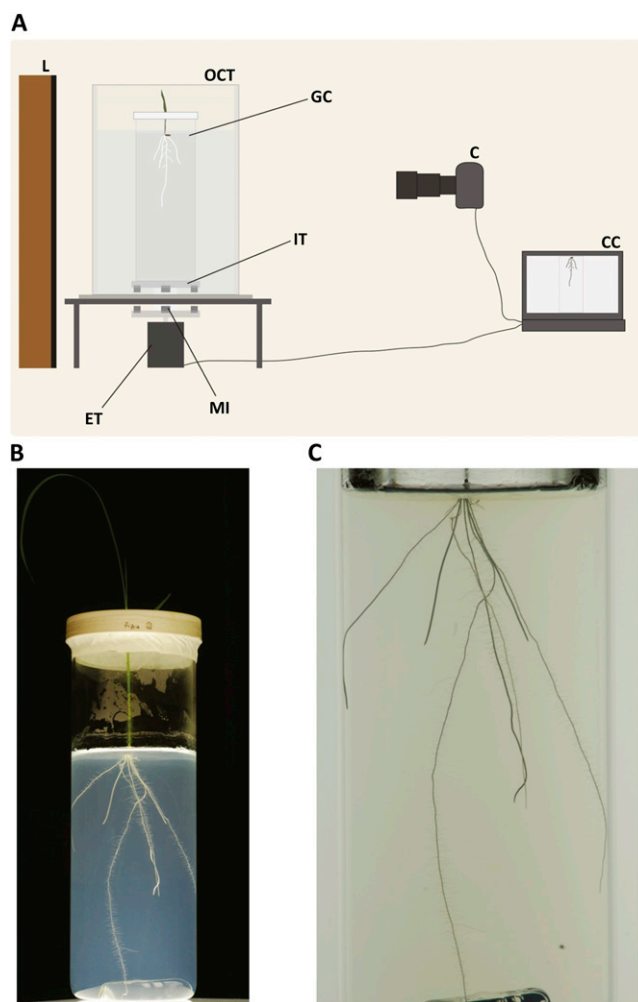


Figure 1. 3D root growth and imaging system. A, Schematic of the 3D imaging system used for capturing image sequences consisting of 40 2D images every 9° of rotation over a full 360° revolution. C, Camera; CC, computer controlling turntable and camera; ET, external turntable; GC, growth cylinder; IT, internal turntable; L, light box; MI, magnetic interface; OCT, optical correction tank. B, Growth cylinder containing gellan gum and a 10-d-old Azucena rice seedling. C, Representative single 2D root system image from an image sequence captured with the 3D imaging system. [See online article for color version of this figure.]

interfaces and mouse and keyboard commands were incorporated into the RootReader3D software to assist in visualizing and interacting with the 3D reconstructions and to facilitate both automated batch analysis of the entire root system and semiautomated modification, separation, selection, labeling, and measurement of individual roots, root components, and zones of interest within the root system (Fig. 2).

Measured Root Traits

The 27 measured root traits calculated with the RootReader3D software can be separated into two categories: static and dynamic root traits. Static root

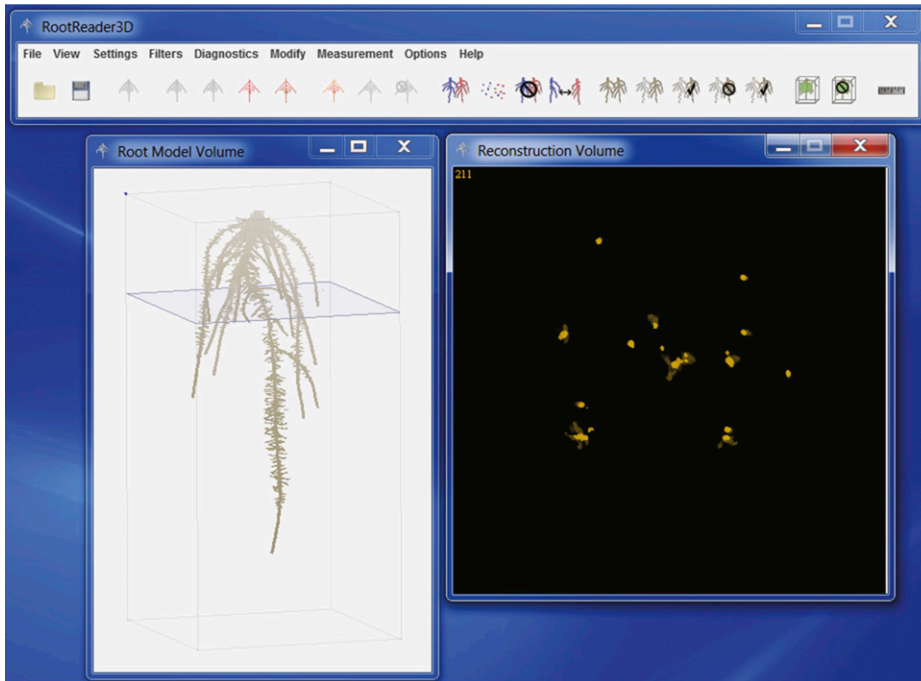


Figure 2. RootReader3D screen shot. RootReader3D software generates high-resolution 3D root system reconstructions from 40 2D images of root systems for plants grown in the gellan gum growth system and also provides the tools to perform both automated and semiautomated trait analysis. The screen shot shows the RootReader3D toolbar (top), the root model volume window (left), and the reconstruction volume window (right) used for visualizing and interacting with the generated 3D root system models. The shaded slice through the 3D root model (left) corresponds to the horizontal cross-section through the root system shown in the reconstruction volume window on the right. [See online article for color version of this figure.]

traits are root characteristics that can be measured at a single point in time, whereas dynamic root traits relate to growth and spatiotemporal changes in root characteristics (de Dorlodot et al., 2007). Static and dynamic traits are not mutually exclusive (i.e. some dynamic traits that describe the growth and development of root systems can be derived from static traits), and both categories can be further subdivided into global and local traits. Global traits are derived from the entire root system or large subsets of the whole system, whereas local traits are derived from individual roots, root classes, or topological zones of interest. The ability to explore a suite of static/dynamic and global/local traits allows for detailed analysis of traditional RSA traits as well as of novel traits that account for developmental changes such as root emergence time and growth characteristics of individual roots and root classes. A list of 3D traits that have been currently integrated into the RootReader3D software, along with further descriptions, explanations, and classifiers for each root trait, are found in Table I.

Root Type Classification

Taking advantage of the phenotyping platform's ability to capture and measure both dynamic and local traits, five specific rice root types can be identified and separated from whole root system reconstructions based on emergence time and visual characteristics, as described by Rebouillat et al. (2009; Fig. 3A). These five root types include the primary root, which develops from the radicle, the embryonic crown roots, the postembryonic crown roots, the large, indeterminate lateral roots, and the small, determinant lateral

roots (Hochholdinger and Tuberosa, 2009). Utilizing the growth rates derived from the daily selection, labeling, and measurement of individual crown root lengths, root emergence time was predicted and the crown roots were separated into embryonic and postembryonic crown root classes, where embryonic and postembryonic crown roots emerged 2 and 6 d after the primary root, respectively (Fig. 3B). The primary root and large lateral roots were identified using visual features such as root length and branching patterns. Once the root types of the entire root systems were classified, root type-specific traits were measured including count (no. of roots), length, growth rate, circumnutation, initiation angle, and gravitropic response (Supplemental Table S1). Additionally, to complement root type classification, the structurally complex and overlapping 10-d root systems can also be algorithmically separated, enabling clearer visualization and the finer analysis of global root system qualities (see Supplemental Video S1, where the crown roots have been digitally separated from the entire root system, allowing further computational analysis of each root system component separately).

Imaging Time Course

To further investigate a variety of static/dynamic and global/local RSA traits, Azucena and IR64 plants were grown and imaged daily for 10 d (Fig. 4). The phenotyping platform enables us to precisely quantify and monitor a number of root growth and RSA traits in both genotypes daily over the 10-d period. As depicted in Figure 5, A and B, it is clear that there are significant differences in RSA when objectively viewing the 3D

Table 1. *Measured root traits*

Root types and processing are as follows: total root system (trs), zone of interest (zoi), primary root (pr), embryonic crown roots (ecr), postembryonic crown roots (pecr), large lateral roots (llr), primary root plus connected lateral roots (pr+), crown roots plus connected lateral roots (cr+), automated (a), and semiautomated (sa).

| Trait | Root Types | Processing | Units | Description |
|-----------------------------|--|------------|----------------------------------|--|
| Length (L) | trs, zoi, pr, ecr, pecr, llr, pr+, cr+ | a, sa | cm | Length along the skeleton of the whole root system, root system component, or root using a polyline length estimation technique |
| Maximum width (MaxW) | trs, pr+, cr+ | a, sa | cm | Maximum horizontal width of the whole root system or root system component measured every 0.2° of rotation |
| Minimum width (MinW) | trs, pr+, cr+ | a, sa | cm | Minimum horizontal width of the whole root system or root system component measured every 0.2° of rotation |
| Maximum depth (MaxD) | trs, pr+, cr+ | a, sa | cm | Maximum vertical depth of the whole root system or root system component measured in relation to the upper-most slice containing a root system voxel |
| MinW/MaxW ratio | trs, pr+, cr+ | a, sa | cm cm ⁻¹ | Ratio of minimum width to maximum width |
| MaxW/MaxD ratio | trs, pr+, cr+ | a, sa | cm cm ⁻¹ | Ratio of maximum width to maximum depth |
| Centroid | trs, pr+, cr+ | a, sa | cm | Vertical position of the center of mass of the entire root system or root system component |
| Exploitation volume | trs, zoi, pr+, cr+ | a, sa | cm ³ | Volume surrounding the root system or root system component at a specified radius minus the root system or root component volume (adapted from Berntson, 1994) |
| Exploitation index | trs, zoi, pr+, cr+ | a, sa | cm ³ cm ⁻¹ | Ratio of the exploitation volume to root system length (adapted from Berntson, 1994) |
| Median no. of roots (MedR) | trs, zoi, pr+, cr+ | a, sa | <i>n</i> | Median no. of roots from root counts taken from all horizontal cross-sectional slices through the entire root system or root system component (adapted from Iyer-Pascuzzi et al., 2010) |
| Maximum no. of roots (MaxR) | trs, zoi, pr+, cr+ | a, sa | <i>n</i> | No. of roots at the 84th percentile of a sorted list (smallest to largest) of root counts from all horizontal cross-sections through the entire root system or root system component (adapted from Iyer-Pascuzzi et al., 2010) |
| MaxR/MedR ratio (bushiness) | trs, zoi, pr+, cr+ | a, sa | <i>n/n</i> | Ratio of the maximum no. of roots to the median no. of roots (adapted from Iyer-Pascuzzi et al., 2010) |
| Surface area (SA) | trs, zoi, pr+, cr+ | a, sa | cm ² | Summed surface area of the whole root system or root system component voxels that are six-connected with a background voxel |
| SA/V ratio | trs, zoi, pr+, cr+ | a, sa | cm ² cm ⁻³ | Ratio of surface area to volume |
| SA/L ratio | trs, zoi, pr+, cr+ | a, sa | cm ² cm ⁻¹ | Ratio of surface area to length |
| Volume distribution | trs | a | cm ³ cm ⁻³ | Ratio of the volume of the root system contained above one-third depth of the root system to the volume of the root system contained below one-third depth of the root system |
| Convex hull volume (CHV) | trs | a | cm ³ | Volume of the convex hull that encompasses the whole root system; the convex hull is found by summing the convex hulls of all horizontal cross-sectional slices through the root system, where the convex hull is the smallest convex set of voxels that contains all other root voxels in the slice (adapted from Iyer-Pascuzzi et al., 2010) |
| V/CHV (solidity) | trs | a | cm ³ cm ⁻³ | Ratio of volume to convex hull volume (adapted from Iyer-Pascuzzi et al., 2010) |
| Emergence time | pr, ecr, pecr, llr | sa | d | Average root emergence time for a given root type in relation to the planting date |
| Initiation angle | pr, ecr, pecr, llr | sa | ° | Average horizontal root initiation angle for a given root type, measured in relation to gellan gum surface or horizontal |
| Gravitropic response | pr, ecr, pecr, llr | sa | ° cm ⁻¹ | Difference in the horizontal root angle divided by the length of the root or root section |

(Table continues on following page.)

Table I. (Continued from previous page.)

| Trait | Root Types | Processing | Units | Description |
|----------------------------|---------------------|------------|---------------------------|--|
| Circumnutation | pr, ecr, pechr, llr | sa | $^{\circ} \text{cm}^{-1}$ | Difference in the root turn angle divided by the length of the root or root section |
| Narrowness index | trs, pr+, cr+ | a, sa | cm cm^{-1} | Average ratio of minimum width to maximum width for each horizontal cross-sectional slice through the whole root system; slices that only contain the primary root and its connected laterals are excluded |
| Volume (V) | trs, zoi, pr+, cr+ | a, sa | cm^3 | Volume of the whole root system or root system component |
| Count | pr, ecr, pechr, llr | sa | n | No. of roots of a particular type |
| Tip count | trs | a | n | No. of root tips in the whole root system, measured from the root system skeleton; this is the no. of skeleton voxels that have only one 26-connected neighbor voxel |
| L/V (specific root length) | trs, zoi, pr+, cr+ | a, sa | cm cm^{-3} | Ratio of length to volume of the whole root system or root system component (adapted from Eissenstat, 1991; Iyer-Pascuzzi et al., 2010) |

reconstructions of the Azucena and IR64 root systems. However, these differences were not detected when the average length of the different root types (primary root, lateral roots, embryonic crown roots, postembryonic crown roots) was quantified in individual Azucena and IR64 seedlings over the 10-d period (Fig. 5, C and D). When traits that describe different aspects of the total RSA were determined, the differences in RSA between Azucena and IR64 could be quantified. Three RSA traits that were significantly different between the two rice genotypes are centroid, volume distribution, and bushiness. Centroid is the vertical position of the center of mass for the entire root system in relation to the seed (Table I). From the top panel of Figure 5D, Azucena has a significantly larger value for its center of mass as early as day 3, indicating that the Azucena root system tends to grow deeper in the gellan gum profile and has less root volume and branching near the top of the root system. Volume distribution is the ratio of the volume occupied by the top one-third of the root system divided by the volume occupied by the bottom two-thirds of the root system. From the middle panel of Figure 5D, IR64 has a considerably larger

volume distribution over the last 4 d of the growth experiment, again indicating that its root system explores the top gellan gum profile more broadly than Azucena. Finally, bushiness, which was first described by Iyer-Pascuzzi et al. (2010), is the ratio of the maximum number of roots divided by median number of roots and can be considered a measure of the global branching complexity of the root system. As seen in the bottom panel of Figure 5D, IR64 has higher bushiness values over days 7 through 10 of the growth experiment, indicating that IR64 has a more highly branched and complex root system. For a complete summary of the analyzed root traits, see Supplemental Table S1.

Validation of 3D Measurements

To validate the root system measurements made by the phenotyping platform, a set of root system traits measured from the reconstructed 3D root models were compared with 2D measurements made on the same root systems using the methods described by Famoso et al. (2010). These traits included primary root length, total root system length, and maximum root system

Table II. Comparison of root traits for plants grown on gellan gum, sand, and hydroponics

Root traits are as follows: primary root length (PRL), in cm; total root length (TRL), in cm; crown root number (CRN); lateral root number (LRN); average crown root length (ACRL), in cm; and average lateral root length (ALRL), in cm.

| Growth System | Condition | Genotype | PRL | TRL | CRN | LRN | ACRL | ALRL |
|---------------|------------|----------|-------------------|--------------------|-------------------|----------------------|------------------|-------------------|
| Gellan gum | – | Azucena | 22.7 | 289.3 | 10.6 | 766.6 | 8.5 | 0.26 |
| Hydroponics | Aerated | Azucena | 23.5 | 277.2 | 8.5 ^a | 797.7 | 8.7 | 0.25 |
| Sand | Aerated | Azucena | 20.5 | 313.4 | 10.1 | 365.6 ^a | 6.4 ^a | 0.62 ^b |
| Hydroponics | Nonaerated | Azucena | 22 | 329.7 | 9.9 | 832.6 | 8.1 | 0.3 |
| Sand | Nonaerated | Azucena | 18.9 ^a | 410.6 ^b | 12.7 | 481.3 ^a | 7.1 ^a | 0.64 ^b |
| Gellan gum | – | IR64 | 15.6 | 289.6 | 15.3 | 743.7 | 6.1 | 0.26 |
| Hydroponics | Aerated | IR64 | 17.3 | 394.7 ^b | 18.8 ^b | 1,010.6 ^b | 5.9 | 0.28 |
| Sand | Aerated | IR64 | 18.6 ^b | 259.3 | 15.1 | 367.8 ^a | 4.8 ^a | 0.46 ^b |
| Hydroponics | Nonaerated | IR64 | 9.4 ^a | 331.4 | 19.2 ^b | 805.7 | 4.6 ^a | 0.29 |
| Sand | Nonaerated | IR64 | 20.7 ^b | 512.8 ^b | 18.2 | 541.4 ^a | 5.7 | 0.71 ^b |

^aSignificant decrease from gellan gum using a *t* test ($P < 0.05$).

^bSignificant increase from gellan gum using a *t* test ($P < 0.05$).

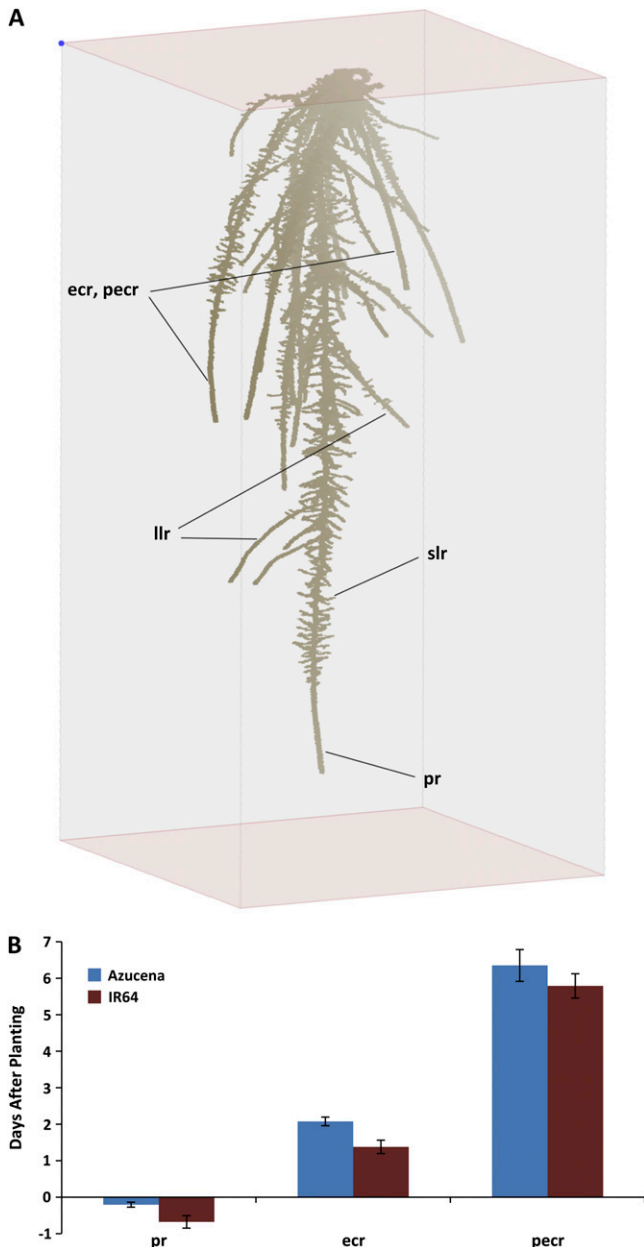


Figure 3. Rice root types. A, Depiction of the five root types: the primary (pr), embryonic crown (ecr), postembryonic crown (pecr), large lateral (llr), and small lateral (slr) roots. As labeled on the 3D root model above, the primary, crown, and large and small lateral roots can be visually distinguished from one another. Temporal imaging is performed to further separate the crown roots into embryonic and postembryonic crown root types based on emergence time. Roots that emerged from the crown between 1 and 5 d after planting were classified as embryonic crown roots, whereas roots that emerged later than 5 d after planting were classified as postembryonic crown roots. B, Average root emergence times of primary and crown roots. Roots were individually selected and measured daily to determine emergence times based on average growth rates. Error bars represent se for all roots of a particular genotype and type. [See online article for color version of this figure.]

width, which were selected to examine the geometric accuracy and consistency of the 3D root reconstruction and measurements made with the RootReader3D software. All traits were found to be significantly correlated ($P < 0.05$) between the 3D and 2D measurement methods (Supplemental Fig. S2), with linear fit estimates of $r^2 = 0.55$, slope = 1.10 for primary root length, $r^2 = 0.91$, slope = 1.54 for total root system length, and $r^2 = 0.99$, slope = 1.05 for maximum root system width.

Comparison of RSA Traits for Plants Grown on the Gellan Gum System Versus Hydroponic and Sand Growth Systems

To evaluate if the gellan gum system had specific impacts on rice root characteristics, 2D root traits were compared between the root systems of plants grown in the gellan gum system versus those of plants grown in hydroponic or sand culture systems under aerated and nonaerated conditions, with identical nutrient, lighting, and temperature regimes (Table II). The set of root traits compared between the three growth systems included primary root length, total root system length, crown root number, lateral root number, average crown root length, and average lateral root length.

Some differences were observed between root growth in gellan gum compared with roots grown in hydroponics and sand, and there were also some genotype-based differences in the root responses. In general, growth of the entire root system and some root types was less in gellan gum compared with the other two growth media, possibly due to slightly less oxygen availability, especially for roots growing deeper in the gellan medium. Surprisingly, the biggest differences were seen between plants grown in the nonaerated sand and the other growth systems. The greatest root growth was seen in the nonaerated sand system compared with plants grown on gellan gum, hydroponics (aerated and nonaerated), and aerated sand. For example, for Azucena seedlings, total root length for plants grown on nonaerated sand was 42% greater than in plants grown in gellan gum, and total root length was 48%, 31%, and 25% greater than in plants grown in aerated hydroponics, aerated sand, and nonaerated hydroponics, respectively. In general, root system characteristics for rice seedlings grown in gellan gum were relatively similar to the same root traits for plants grown in hydroponics and aerated sand culture, and the root systems of plants grown on all of these growth systems grew less vigorously than for plants grown on nonaerated sand.

DISCUSSION

Exploring the Development of Whole Root Systems by Root Types

While developing the platform to expand the throughput and phenotyping capability of 3D RSA trait analysis, it was found that many additional

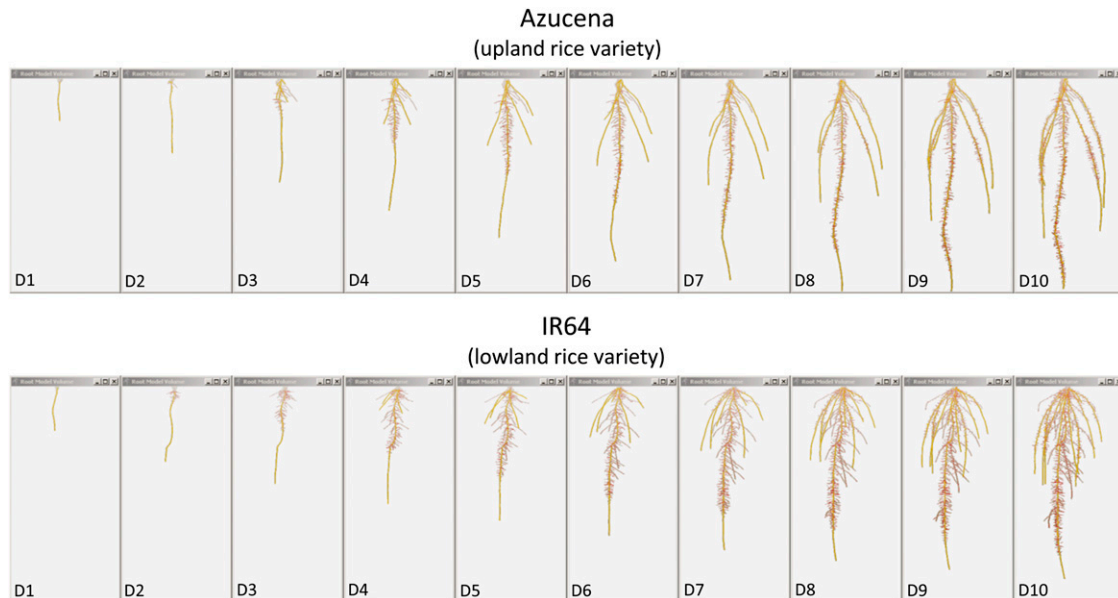


Figure 4. 3D root system models generated from daily imaging of root systems over a 10-d period using the RootReader3D software (day 1 [D1]–day 10 [D10]). The skeletons of the root systems are shown in red, and the primary and crown roots are shown in yellow. The primary and crown roots were selected and labeled, allowing for dynamic tracking of root type-specific growth features.

aspects of root systems could also be explored. One novel feature of the platform is the ability to identify and classify five different rice root types from whole root system reconstructions.

As with other monocot species, the rice root system is largely composed of a fibrous network of embryonic and postembryonic roots. In monocots, the rapid elongation and lateral root establishment of the primary and embryonic crown roots is critical for early seedling vigor, whereas postembryonic crown roots become increasingly important during further plant growth (Hochholdinger and Tuberosa, 2009). Additionally, through mutant analysis studies in rice, it has been found that these root types are controlled by distinctly different genetic and developmental networks (Hochholdinger et al., 2004; Rebouillat et al., 2009). The ability of this root imaging and analysis platform to separate and track the growth features of these five root types individually can help detect and further characterize the genetic and developmental changes that occur as the root system develops and the plant matures.

Using 3D Information to Further Investigate Root Traits

Building upon root type classification, the 3D information provided by the root reconstructions can also be used to investigate traits that have only been studied using 2D analysis systems. Two traits that can be enhanced by utilizing root type and 3D information are root circumnutation and gravitropism. Root circumnutation describes the tendency of roots to grow downward through their growth medium along a

helical axis and has been mainly studied by analyzing the skewing and periodic waving patterns of the primary roots of *Arabidopsis* (*Arabidopsis thaliana*) plants grown on 2D agar plate systems. While the causes of the observed skewing and waving patterns remain under debate, at present they have mainly been attributed to three intrinsic growth responses, circumnutation, gravitropism, and negative thigmotropism (Migliaccio and Piconese, 2001; Oliva and Dunand, 2007), and are suggested to be linked with the recent discovery of oscillating gene expression cycles that also impact the periodic establishment of lateral root prebranching sites along the primary root of *Arabidopsis* (Moreno-Risueno et al., 2010).

Using the 3D visualization and quantification capabilities of the phenotyping platform, comprehensive investigations into root circumnutation can be extended into rice, a model monocot crop species. Circumnutation was measured on day-10 root system models with RootReader3D (Fig. 6A), where positive values represent a left-handed rotation and negative values represent a right-handed rotation. Circumnutation is measured as the change in tangential angle along the root divided by the length of the measured root section, $(\rho_{\text{fin}} - \rho_{\text{init}})/L$, where ρ_{init} is 0° and ρ_{fin} may be greater than 360° . Although more detailed studies are needed, root circumnutation is present in rice, but it does not vary between Azucena and IR64 genotypes; however, it appears to vary significantly ($P < 0.05$) between different root types (Fig. 6B).

Additionally, the gravitropic response of roots to grow along the gravity vector can also be measured on the different root types. Root gravitropism describes

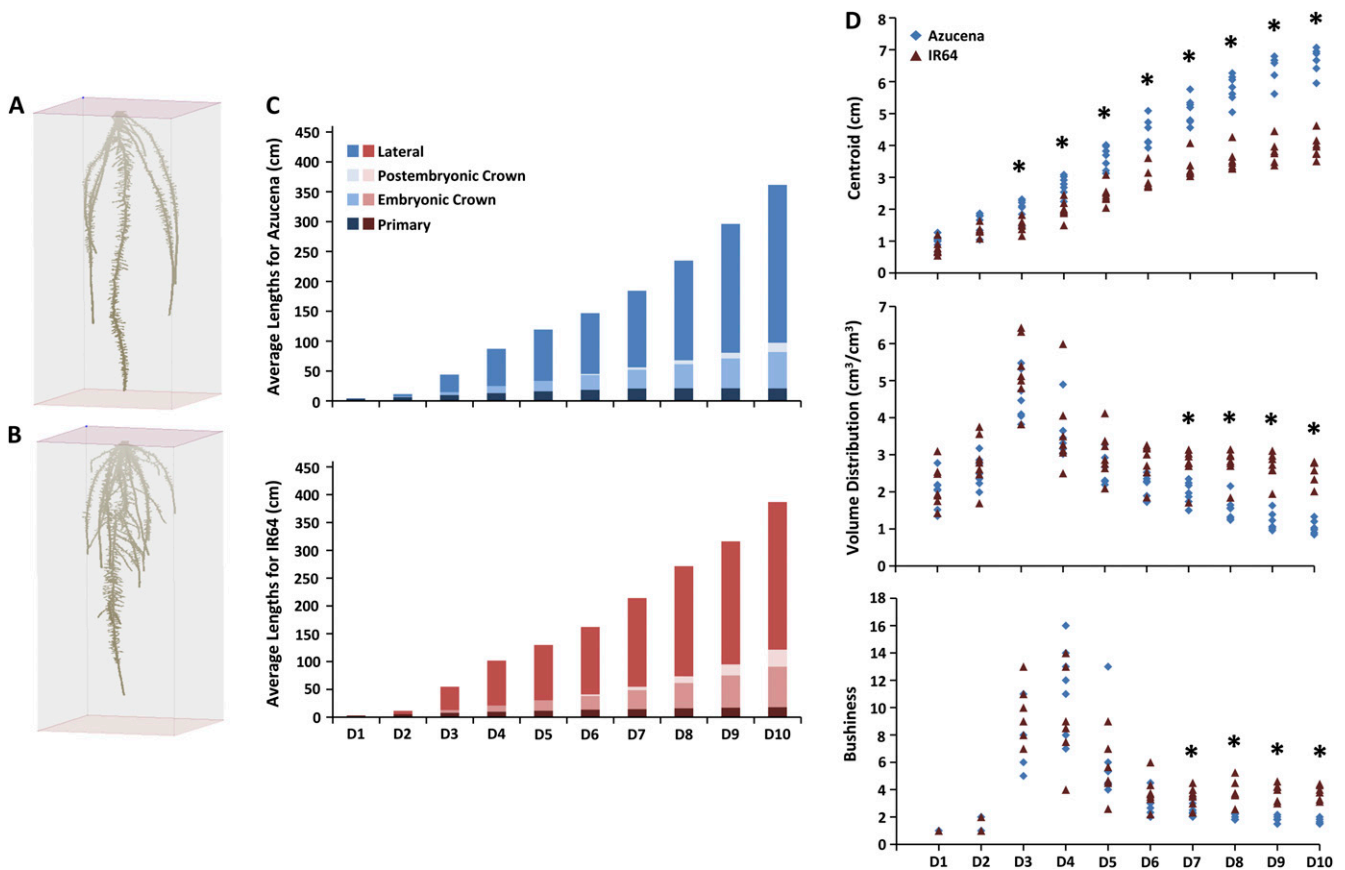


Figure 5. Quantitative description of Azucena and IR64 root system differences. A, Day-10 Azucena 3D root system reconstruction. B, Day-10 IR64 3D root system reconstruction. C, Average root length for different root types for Azucena (blue) and IR64 (red) plants, day 1 (D1) to day 10 (D10); $n = 7$. D, A subset of quantified RSA traits, vertical centroid position, volume distribution, and bushiness, that quantitatively describe the differences between Azucena and IR64 RSA. Each data point represents a single measurement made on an individual Azucena (blue diamonds) or IR64 (red triangles) plant on a given day. Asterisks indicate where significant differences were detected between Azucena and IR64 genotypes using a t test ($P < 0.05$). Volume distribution and bushiness traits were adapted to 3D from 2D methods described by Iyer-Pascuzzi et al. (2010).

the tendency of plant roots to detect and grow downward along the vertical vector force of gravity. In the context of RSA, the initiation angles combined with the gravitropic responses of individual roots can impact the spatial distribution of the entire root system and can ultimately influence the capability of a plant to access and acquire water and nutrient resources.

Both root initiation angle, θ_{init} , and gravitropic response were measured on day-10 root system models, where the initiation angles were measured 5 mm from the basal end of the roots in relation to horizontal (or the gellan gum surface) and the gravitropic response was measured as the change in the tangential angle along the root divided by the length of the measured root section, $(\theta_{\text{fin}} - \theta_{\text{init}})/L$. θ_{fin} and L were measured from the root tip or where the tangential angle to the root reached 75° (Fig. 7A). When investigating the initiation angles of the embryonic crown, the postembryonic crown, and large lateral roots, it was found that root initiation angle did not vary between geno-

types; however, it varied between root types. Additionally, the gravitropic responses of the embryonic crown and large lateral roots were found to be significantly higher for IR64 ($P < 0.05$; Fig. 7B).

Environmental Considerations of Rice Root Traits

Domesticated Asian rice has a complex cultivation history and is raised under a variety of field practices and conditions, ranging from highly managed paddies to unmanaged fields (Sweeney and McCouch, 2007). The two rice varieties used in this study, Azucena and IR64, were selected to represent varieties adapted to different cultivation systems. Azucena, an upland, *tropical japonica* rice, has been adapted for growth under nonirrigated field conditions, whereas IR64, a lowland *indica* rice, has been bred for maximal yields in flooded paddy systems. The deeper rooting behavior of Azucena compared with IR64, when grown in the gellan gum system (Figs. 4 and 5), is consistent

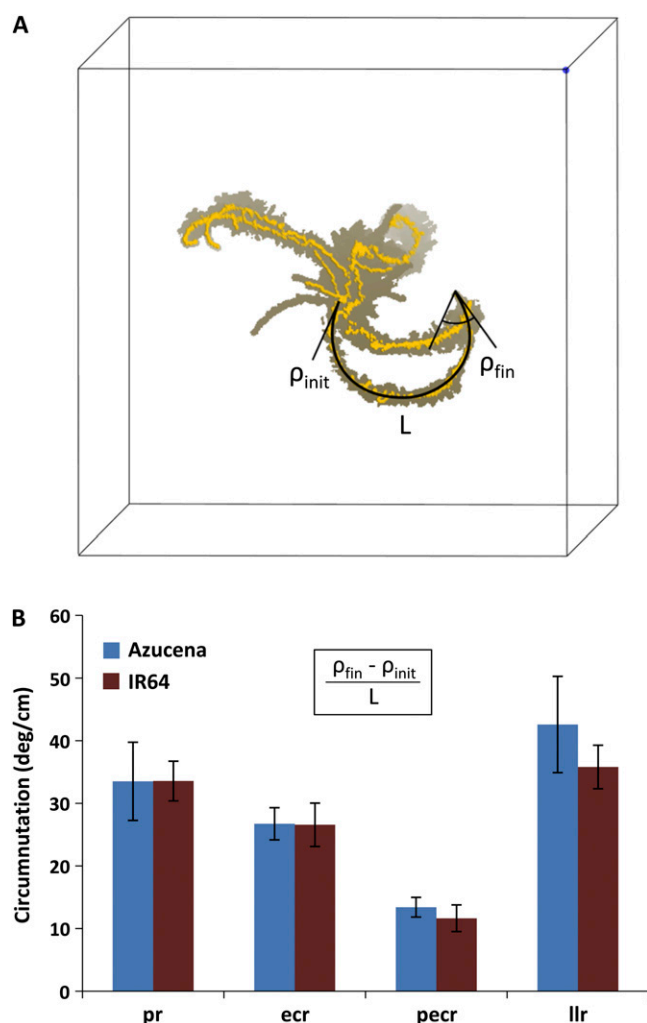


Figure 6. Root circumnutation. A, Top view of a 10-d Azucena root system reconstruction showing tangential angles (ρ_{init} and ρ_{fin}) and root segment length (L) used for measuring circumnutation. Yellow lines are the selected primary and crown roots. B, Average circumnutation rates for different root types for Azucena and IR64 genotypes. Root types are abbreviated as pr (primary root), ecr (embryonic crown roots), peocr (postembryonic crown roots), and llr (large lateral roots). Error bars represent \pm SE for all roots of a particular genotype and type.

with observations made from soil studies (Yadav et al., 1997). However, as expected of varieties selected under varying cultivation practices, when either of these genotypes is subjected to different growth environments, in this case gellan gum versus aerated or non-aerated hydroponic and sand systems, changes in root traits can be dramatic and varied (Table II). This variability demonstrates the complexity of rice root systems and reinforces the idea that adaptive responses to environmental changes can be genotype specific (Nicotra et al., 2010). Additionally, it also suggests that within a plant species, there remains a certain level of plasticity in root traits that could possibly be used to further improve plant performance on diverse agricultural systems.

CONCLUSION

The 3D imaging and RootReader3D software platform described in this paper is a unique imaging and analysis package for investigating both static and dynamic 3D RSA characteristics of plant root systems that have been formerly difficult to measure with high throughput, accuracy, and resolution. The automated and interactive features of RootReader3D also provide a flexible foundation for more extensive root trait analysis in the future. The 27 measured root traits demonstrate the platform's utility for analyzing root systems; however, many root traits and quantitative techniques, including advanced dynamic and topological analyses, have not yet been incorporated into the software to better describe and analyze the 3D root models. The presence of significant differences in basic 2D root traits between gellan gum, hydroponic, and sand growth systems reinforces the fact that plant root systems are highly responsive to their growth environment and that more in-depth evaluation is needed before gellan gum root traits can be directly related to performance under field conditions. The enhanced quantification capabilities and capacity to image over 100 root systems per day, combined with a rapidly advancing array of genetic resources, present many opportunities for dissecting the genetic control and developmental changes of RSA as well as opportunities to explore RSA variation within and between species grown under a range of controlled environmental conditions.

MATERIALS AND METHODS

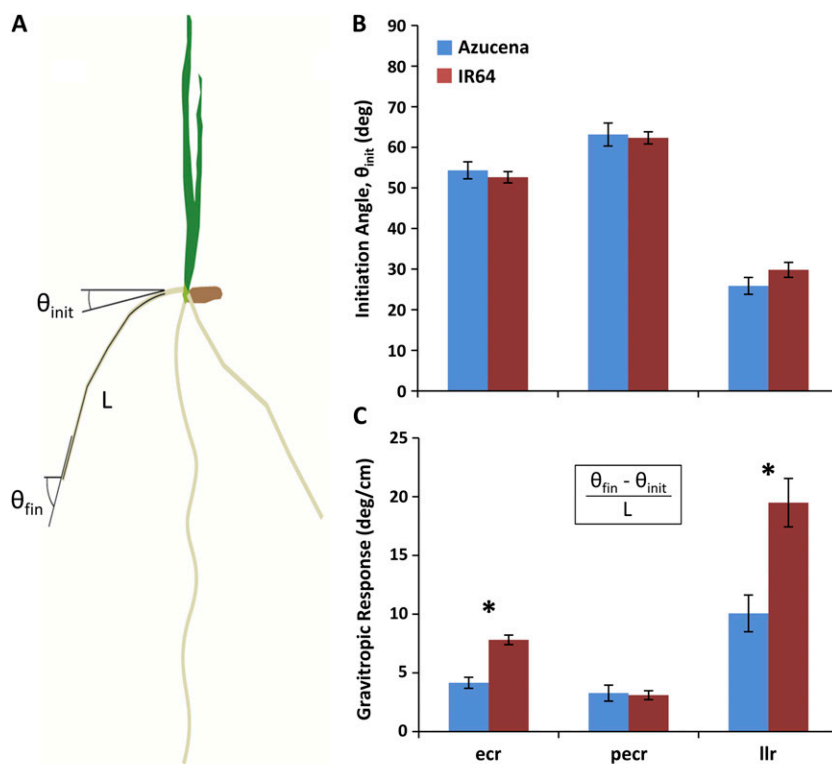
Plant Material and Growth Conditions

Rice (*Oryza sativa*) genotypes Azucena (upland, *tropical japonica*, CIRAD no. 8496) and IR64 (lowland, *indica*, CIRAD no. 8531) were used in this study. The hulls of the seeds were removed, and the seeds were surface sterilized by soaking them in a solution of 70% ethanol for 1 min followed by a solution of 3% sodium hypochlorite for 30 min. The sodium hypochlorite was removed by washing the seeds with sterile 18-M water for a minimum of five rinses. Seeds were germinated in the dark at 30°C on vertically oriented, sterile petri plates with moist filter paper covering the seeds for gellan gum studies or in moist germination paper rolls (Anchor Paper) for hydroponic and sand culture studies.

For gellan gum growth studies, when the emerging radicle had reached approximately 1 cm in length, the sterile seedlings were transplanted into glass growth cylinders (90 mm i.d.; MicroGlass) that contained 1.3 L of modified Magnavaca's growth medium (Famoso et al., 2010) at pH 5.5 that has been solidified with gellan gum (Sigma-Aldrich Phytigel). The gellan gum growth medium was prepared by dissolving and autoclaving 1.95 g of Phytigel powder in 0.65 L of 18-M water. The sterile gellan gum solution was then combined with 0.65 L of 2 \times modified Magnavaca's solution that had been adjusted to pH 6.0 and filter sterilized. The 2 \times modified Magnavaca's solution contained the following: 2.6 mM CaCl₂, 2.0 mM KCl, 3.0 mM NH₄NO₃, 0.4 mM MgSO₄, 1.0 mM Mg(NO₃)₂, 0.91 mM MgCl₂, 200 μ M KH₂PO₄, 154 μ M Fe-HEDTA, 18.2 μ M MnCl₂, 50.8 μ M H₃BO₃, 4.7 μ M ZnSO₄, 1.2 μ M CuSO₄, and 1.7 μ M Na₂MoO₄.

For hydroponic and sand culture studies, when the radicle had grown to 1 to 2 cm in length, the seedlings were transplanted into either aerated or nonaerated hydroponic or sand growth systems containing full-strength modified Magnavaca's solution, pH 5.5. For hydroponics studies, the seedlings were planted into hydroponic growth systems as described by Famoso et al. (2010). The aerated and nonaerated solutions were either continuously

Figure 7. Root gravitropism. A, Depiction of a rice seedling with tangential angles (θ_{init} and θ_{fin}) and root segment length (L) used for measuring gravitropic traits. B, Average root initiation angle (θ_{init}) separated by root type. Root types are abbreviated as pr (primary root), ecr (embryonic crown roots), pecr (postembryonic crown roots), and llr (large lateral roots). C, Gravitropic responses for different root types. Error bars represent \pm SE for all roots of a particular genotype and type. Asterisks indicate where significant differences were detected between Azucena and IR64 genotypes using a *t* test ($P < 0.05$). [See online article for color version of this figure.]



bubbled with filtered air or left stagnant. For sand culture studies, a custom ebb-and-flow growth system was designed where individual plants were grown in 10-cm-diameter \times 30-cm-tall PVC columns filled with sand (Flint Silica no. 12; U.S. Silica) that had been sterilized with 70% ethanol and rinsed with pure water several times. This system involves flooding the sand cylinders up to the sand surface with Magnavaca's solution and then allowing it to drain on a 4-h cycle for aerated plants or continuously flooding the cylinders for the nonaerated plants.

For all three studies, seedlings were grown in a growth chamber for 10 d at 30°C day/26°C night, 12-h/12-h light/dark photoperiod, and 550 $\mu\text{mol m}^{-2} \text{s}^{-1}$ photon flux.

3D Imaging System and Calibration

The 3D imaging system (Fig. 1A) consists of a Nikon D300s Digital SLR camera with a Nikon 180mm f/2.8D AF ED-IF lens placed on a tripod with manual capture settings of 1/30th-s shutter speed, f/22 f-stop, and 200 ISO. The camera was aligned transverse to a custom-developed optical correction tank that was placed 2 m from the center of the turntable in order to minimize potential reconstruction artifacts resulting from the perspective geometry of the imaging system (R.T. Clark, R.B. MacCurdy, and L.V. Kochian, unpublished data). A rectangular optical correction tank was filled with water and incorporated into the imaging system to correct for optical refraction from the curved surface of the glass cylinder (Supplemental Fig. S3). The optical correction tank contained an internal turntable that was magnetically interfaced with an external electronic turntable (model 5718; Lin Engineering). A light box (model BL1824; Hall Productions) was placed behind the correction tank, opposite the camera, providing near-uniform backlighting. Daily image sequences were captured for each plant root system grown in gellan gum, consisting of 40 silhouette images taken every 9° over the entire 360° of rotation and stored using LabVIEW and Nikon Camera Control Pro 2 software (Fig. 1, B and C). Individual image sequences were captured in 4 min, with an image resolution of 50 μm per pixel.

An axis of rotation (AOR) calibration technique was developed to determine the orientation of the AOR in relation to the camera. The AOR was determined by placing an indexed rod on the top-outside edge of the internal turntable and capturing a 2D image sequence over 360° of rotation. The

rotational path of each known index mark was tracked, and three AOR calibration parameters used during reconstruction (translation, roll, and pitch) were calculated from the tracked marks (Supplemental Fig. S4). The scale of reconstruction space, in millimeters per voxel, was determined by measuring the pixel distance between the index marks when the rod was aligned in the imaging plane using ImageJ software (<http://rsb.info.nih.gov/ij/>).

Image Processing and 3D Reconstruction with RootReader3D

Prior to reconstruction, the 2D sequence images were identically cropped, down sampled to a resolution of 200 μm per pixel, and converted to grayscale using Adobe Photoshop (Adobe Systems) to produce images with dark roots surrounded by a bright background. The image sequences were then thresholded, reconstructed, and analyzed using our custom RootReader3D software (www.plantmineralnutrition.net). The root system reconstructions generated with RootReader3D had the same resolution as the preprocessed image sequences.

Validation of Quantification

After image sequences of the 14 10-d-old rice seedlings (seven Azucena and seven IR64 seedlings) were captured, the rice seedlings were removed from the gellan gum growth containers and rinsed. The root systems were excised from the shoot base, spread in the specimen/imaging tray, photographed, and measured with RootReader2D using methods described by Famoso et al. (2010). Primary root and total root system length measurements obtained from RootReader3D software were compared with RootReader2D primary root and total root system length measurements. Maximum root system widths were then determined from the original images using ImageJ and compared with RootReader3D width measurements.

Supplemental Data

The following materials are available in the online version of this article.

Supplemental Figure S1. Depiction of the silhouette-based back-projection and cross-sectional volume segmentation process used by RootReader3D during the generation of 3D root models.

Supplemental Figure S2. 3D measurements versus 2D measurements.

Supplemental Figure S3. Schematic of cylindrical distortion correction.

Supplemental Figure S4. AOR calibration technique.

Supplemental Table S1. Summary of the calculated RSA traits for Azucena and IR64 plants used in the day growth experiment for which specific data sets are shown in Figures 4 and 5 and Table II.

Supplemental Video S1. Movie showing the computationally separated primary and crown root components for subsequent calculation of RSA traits for these dissected root types.

ACKNOWLEDGMENTS

We thank Prof. Anthony P. Reeves for his discussions and lessons on image processing, automated analysis, and the importance of technique validation, William A. Shaben and Douglas B. Caveney for their advice and guidance throughout the system design and fabrication process, and Prof. Xiaolong Yan, Prof. Hong Liao, and Dr. Suqin Fang for providing foundation and insight into 3D reconstruction and RSA. We also thank Brigitte Courtois, Nour Ahmadi, and Dominique This for providing the Azucena and IR64 seeds used during the root growth studies.

Received November 9, 2010; accepted March 22, 2011; published March 31, 2011.

LITERATURE CITED

- Armengaud P, Zambaux K, Hills A, Sulpice R, Pattison RJ, Blatt MR, Amtmann A (2009) EZ-Rhizo: integrated software for the fast and accurate measurement of root system architecture. *Plant J* **57**: 945–956
- Berntson GM (1994) Modelling root architecture: are there tradeoffs between efficiency and potential of resource acquisition? *New Phytol* **127**: 483–493
- de Dorlodot S, Forster B, Pagès L, Price A, Tuberosa R, Draye X (2007) Root system architecture: opportunities and constraints for genetic improvement of crops. *Trends Plant Sci* **12**: 474–481
- Eissenstat DM (1991) On the relationship between specific root length and rate of root proliferation: a field study using citrus rootstocks. *New Phytol* **118**: 63–68
- Famoso AN, Clark RT, Shaff JE, Craft E, McCouch SR, Kochian LV (2010) Development of a novel aluminum tolerance phenotyping platform used for comparisons of cereal aluminum tolerance and investigations into rice aluminum tolerance mechanisms. *Plant Physiol* **153**: 1678–1691
- Fang S, Yan X, Liao H (2009) 3D reconstruction and dynamic modeling of root architecture in situ and its application to crop phosphorus research. *Plant J* **60**: 1096–1108
- Gregory PJ, Hutchison DJ, Read DB, Jenneson PM, Gilboy WB, Morton EJ (2003) Non-invasive imaging of roots with high resolution X-ray micro-tomography. *Plant Soil* **255**: 351–359
- Ho MD, McCannon BC, Lynch JP (2004) Optimization modeling of plant root architecture for water and phosphorus acquisition. *J Theor Biol* **226**: 331–340
- Hochholdinger F, Park WJ, Sauer M, Woll K (2004) From weeds to crops: genetic analysis of root development in cereals. *Trends Plant Sci* **9**: 42–48
- Hochholdinger F, Tuberosa R (2009) Genetic and genomic dissection of maize root development and architecture. *Curr Opin Plant Biol* **12**: 172–177
- Iyer-Pascuzzi AS, Symonova O, Mileyko Y, Hao Y, Belcher H, Harer J, Weitz JS, Benfey PN (2010) Imaging and analysis platform for automatic phenotyping and trait ranking of plant root systems. *Plant Physiol* **152**: 1148–1157
- Kalman P, Attila K (1999) A parallel 3D 12-subiteration thinning algorithm. *Graph Models Image Process* **61**: 199–221
- Liao H, Rubio G, Yan X, Cao A, Brown KM, Lynch JP (2001) Effect of phosphorus availability on basal root shallowness in common bean. *Plant Soil* **232**: 69–79
- Liu H, Wang S, Yu X, Yu J, He X, Zhang S, Shou H, Wu P (2005) ARL1, a LOB-domain protein required for adventitious root formation in rice. *Plant J* **43**: 47–56
- Lynch J (1995) Root architecture and plant productivity. *Plant Physiol* **109**: 7–13
- Malamy JE (2005) Intrinsic and environmental response pathways that regulate root system architecture. *Plant Cell Environ* **28**: 67–77
- Migliaccio F, Piconese S (2001) Spiralizations and tropisms in Arabidopsis roots. *Trends Plant Sci* **6**: 561–565
- Moreno-Risueno MA, Van Norman JM, Moreno A, Zhang J, Ahnert SE, Benfey PN (2010) Oscillating gene expression determines competence for periodic Arabidopsis root branching. *Science* **329**: 1306–1311
- Mulayim AY, Yilmaz U, Atalay V (2003) Silhouette-based 3D model reconstruction from multiple images. *IEEE Trans Syst Man Cybern B Cybern* **33**: 582–591
- Nicotra AB, Atkin OK, Bonser SP, Davidson AM, Finnegan EJ, Mathesius U, Poot P, Purugganan MD, Richards CL, Valladares F, et al (2010) Plant phenotypic plasticity in a changing climate. *Trends Plant Sci* **15**: 684–692
- Oliva M, Dunand C (2007) Waving and skewing: how gravity and the surface of growth media affect root development in Arabidopsis. *New Phytol* **176**: 37–43
- Rebouillat J, Dievart A, Verdeil J, Escoute J, Giese G, Breitler J, Gantet P, Espeout S, Guiderdoni E, Périn C (2009) Molecular genetics of rice root development. *Rice* **2**: 15–34
- Ribaut J-M, Betran J, Monneveux P, Setter T (2009) Drought tolerance in maize. In JL Bennetzen, SC Hake, eds, *Handbook of Maize: Its Biology*. Springer, New York, pp 311–344
- Shaff J, Schultz B, Craft E, Clark R, Kochian L (2009) GEOCHEM-EZ: a chemical speciation program with greater power and flexibility. *Plant Soil* **303**: 207–214
- Smit AL (2000) *Root Methods: A Handbook*. Springer, Berlin
- Sweeney M, McCouch S (2007) The complex history of the domestication of rice. *Ann Bot (Lond)* **100**: 951–957
- Taylor HM, Upchurch DR, McMichael BL (1990) Applications and limitations of rhizotrons and minirhizotrons for root studies. *Plant Soil* **129**: 29–35
- Trachsel S, Kaeppeler SM, Brown KM, Lynch JP (2011) Shovelomics: high throughput phenotyping of maize (*Zea mays* L.) root architecture in the field. *Plant Soil* **341**: 75–87
- Tracy SR, Roberts JA, Black CR, McNeill A, Davidson R, Mooney SJ (2010) The X-factor: visualizing undisturbed root architecture in soils using X-ray computed tomography. *J Exp Bot* **61**: 311–313
- Tuberosa R, Salvi S (2006) Genomics-based approaches to improve drought tolerance of crops. *Trends Plant Sci* **11**: 405–412
- Wang T, Cheng I (2008) Generation of unit-width curve skeletons based on valence driven spatial median (VDSM). In G Bebis, R Boyle, B Parvin, D Koracin, P Remagnino, F Porikli, J Peters, J Klosowski, L Arns, YK Chun, T Rhyne, L Monroe, eds, *Lecture Notes in Computer Science, Advances in Visual Computing, Vol 5358*. Springer, Berlin, pp 1051–1060
- Ward JT, Lahner B, Yakubova E, Salt DE, Raghothama KG (2008) The effect of iron on the primary root elongation of Arabidopsis during phosphate deficiency. *Plant Physiol* **147**: 1181–1191
- Yadav R, Courtois B, Huang N, McLaren G (1997) Mapping genes controlling root morphology and root distribution in a doubled-haploid population of rice. *Theor Appl Genet* **94**: 619–632
- Zhu J, Kaeppeler SM, Lynch JP (2005) Topsoil foraging and phosphorus acquisition efficiency in maize (*Zea mays*). *Funct Plant Biol* **32**: 749–762
- Zhu T, Fang S, Li Z, Liu Y, Liao H, Yan X (2006) Quantitative analysis of 3-dimensional root architecture based on image reconstruction and its application to research on phosphorus uptake in soybean. *Chin Sci Bull* **51**: 2351–2361